Effect of Errors in Reangulation on Planar and Tomographic Thallium-201 Washout Profile Curves

Jack L. Lancaster, Mark R. Starling*, David T. Kopp, John C. Lasher, and Ralph Blumhardt

Department of Radiology, Nuclear Medicine Division, The University of Texas Health Science Center at San Antonio, Texas

Cardiac phantom studies were performed with and without a defect present to test the hypothesis that myocardial ^{201}Tl quantitative circumferential washout profile curves calculated from planar and rotating slant hole (RSH) collimator tomographic images are equally affected by errors in axial repositioning. Simulated stress images were acquired with the long axis of the phantom perpendicular to the camera surface and redistribution images were acquired to represent 50% ^{201}Tl washout with axial repositioning errors relative to the stress position ranging from 0 to 20° in 5° increments. There was a decrease in the ^{201}Tl washout profile curves compared to that expected (50%) in the wall tilted away from the camera surface, and a reciprocal increase in the ^{201}Tl washout profile curves in the wall tilted towards the camera surface for both imaging techniques whether a lesion was present or not. This effect became more pronounced as the error in axial repositioning was increased for both the planar ($p < 0.001$) and the RSH tomographic ($p < 0.001$) techniques. However, the deviation of the ^{201}Tl washout profile curves from that expected (50%) was greater for the planar imaging technique with or without a lesion ($p < 0.05$ to 0.001). Thus, we conclude that ^{201}Tl quantitative circumferential washout profile curves calculated using this tomographic imaging technique are less affected by errors in axial repositioning than those calculated using an equivalent projection by standard planar imaging methods. These data emphasize the importance which must be placed on the repositioning of patients to obtain valid ^{201}Tl washout profile curves for the detection and localization of coronary artery disease.

J Nucl Med 26:1445–1455, 1985

Qualitative planar thallium-201 (^{201}Tl) myocardial scintigraphy has improved the detection of coronary artery disease (CAD) compared to electrocardiographic evidence for myocardial ischemia during treadmill exercise testing (*1–8*). Quantitative planar techniques employing myocardial ^{201}Tl washout profile curves have further increased the detection of CAD, particularly multivessel disease, compared to a qualitative interpretation of the planar ^{201}Tl images (*9–12*). An alternative method to planar myocardial scintigraphy is that of tomography, which has been reported to detect CAD with a high degree of sensitivity and specificity (*13–22*). A critical assumption with myocardial ^{201}Tl quantitative washout profile curves derived from planar or tomographic images is that the position of the heart during the stress and redistribution acquisitions is precisely the same; and, thus, time and ^{201}Tl redistribution will be the only variables between acquisitions. Although myocardial ^{201}Tl activity can be easily centered in the image for each method of image acquisition, this does not assure accurate realignment in the axial direction. However, no data are available which compare the relative effects of repositioning errors on myocardial ^{201}Tl quantitative washout profile curves generated from planar and tomographic imaging techniques.

Received July 11, 1985; revision accepted Aug. 2, 1985.

For reprints contact: Jack L. Lancaster, PhD, Dept. of Radiology, Nuclear Medicine Div. The University of Texas HSCSA, 7703 Floyd Curl Dr., San Antonio, TX 78284.

*Present address: Dept. of Medicine, Division of Cardiology, VA Medical Center, Ann Arbor, MI.

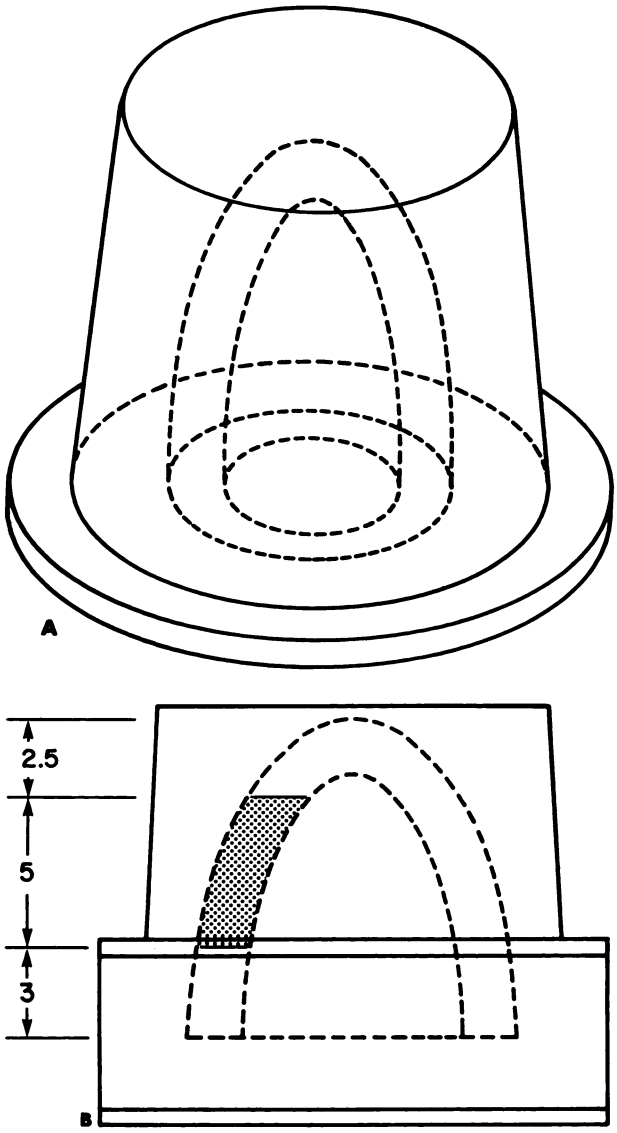

FIGURE 1
A: Heart phantom (see text). B: Heart phantom with lesion in place. Approximate dimensions in cm are indicated

Thus, we tested the hypothesis that ^{201}Tl circumferential washout profile curves calculated from simulated stress and redistribution myocardial ^{201}Tl images using a heart phantom with planar and rotating slant hole collimator tomographic imaging techniques are equally affected by errors in axial repositioning between the simulated stress and redistribution acquisitions.

MATERIALS AND METHODS

Heart phantom

The plastic heart phantom* is schematically represented in Fig. 1. It consists of an outer conically shaped container and similarly shaped smaller inner plug, which provides a 1.0-cm-thick space to simulate the myocardium. This space was filled with an aqueous solution containing ^{201}Tl (0.3 mCi, 11.1 MBq). Residual air was evacuated through the filing port in order to eliminate bubble artifacts. The dimensions of the sealed aqueous solution at the base of the heart phantom consisted of a 5-cm inner diameter and a 7-cm outer diameter with a length from the base to the apex of 8.5 cm. The phantom was immersed in a cylinder of water to simulate human tissue attenuation. The heart phantom was positioned within the cylinder of water so that its apex was in contact with and its long axis was perpendicular to the cylinder wall. A plastic plug measuring 5.4 cm in length, 1.0 cm thick, and 2.5 cm wide was positioned within the phantom wall prior to some of the serial acquisitions to simulate a myocardial defect parallel to the long axis (Fig. 1, Panel B). Images of the phantom were acquired utilizing both planar and tomographic methods for three configurations of the phantom: (1) no lesion, (2) lesion top, and (3) lesion side.

Planar image acquisition

Planar images were acquired with a gamma camera† using a low-energy, parallel channel collimator. Dual energy windows of 20% were centered on the 70 keV mercury x-ray peak and the 167-keV gamma peak of ^{201}Tl.

The heart phantom was initially positioned with the base of the phantom parallel to the gamma camera collimator. Positioning was aided using a level/angle measuring device accurate to 1/2 degree. The collimator face and phantom base were oriented such that their surfaces were parallel to within 1/2 degree; and, thus, the long axis of the phantom was initially perpendicular to the collimator face. The collimator was facing and 2.5 cm from the apex of the phantom. Positioning of the 0° reference images was guided by inspection of preliminary stress and redistribution profile curves. At this position images were acquired using a zoom factor of 1.48. A total of 500k counts per image were obtained with the phantom at 0° and tilted at 5, 10, 15, and 20° relative to the initial 0° position. A stress image was generated by multiplying the 0° image by a factor of two. Thus, the ^{201}Tl activity in the redistribution images at 0° and at each angle of mispositioning should be equivalent to one-half that in the simulated stress image. The phantom was positioned to maintain image centering for the 5 to 20° reangulation images. A computer‡ was used to acquire images into a 64 × 64 word mode matrix. The total acquisition time for the planar data was less than 20 min.

Tomographic image acquisition

Tomographic images were acquired with a large field-of-view gamma camera§ equipped with a 30° bilateral rotating slant hole (RSH) collimator.* Three 20% energy windows were centered on the 70 keV mercury x-ray peak and the 135 and 167 keV gamma peaks of ^{201}Tl. No zoom was used for tomographic image acquisition. This

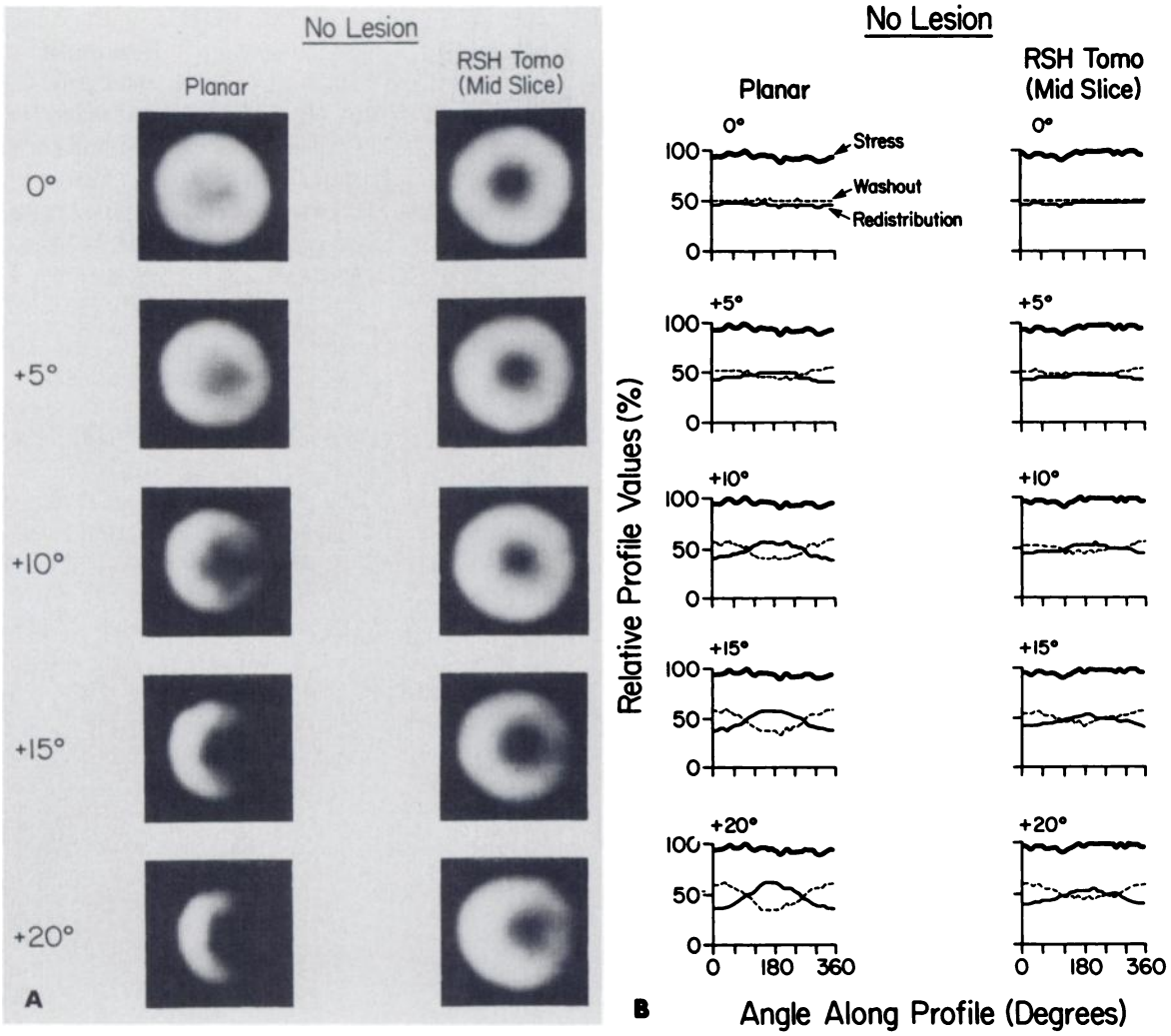

FIGURE 2

A: Planar and RSH tomographic (mid-slice) images of heart phantom containing ^{201}Tl with no lesion are shown. Angles indicate tilt about vertical axis relative to 0° image. Positive tilt angles are such that right side of phantom (as viewed from the camera) is tilted towards gamma camera. This results in decreased counts per unit area on right side with a progressively greater decrease as tilt angle increases. Both planar and RSH tomographic images were smoothed once prior to taking the photographs. Film exposure factors were selected to emphasize the effects of tilting the cardiac phantom away from 0° orientation. Identical exposure factors were used for both the planar and RSH images. These exposure factors yielded photographs which differed somewhat from actual image appearance.

B: Planar and RSH tomographic (mid-slice) stress, redistribution, and washout profile curves from images in Fig. 2A are shown. Curves are relative profile values with 0° profile angle representing right side (or three o'clock) and proceeding around images in counterclockwise direction to 359°. With this profile angle labeling scheme, 0° represents the right, 90° top, 180° the left, and 270° bottom of images from Fig. 2A

yielded reconstructed images which were approximately the same size as the planar images.

Positioning of the phantom for imaging was as described for the planar image acquisitions. Imaging with the CMS bilateral RSH collimator involved acquiring two simultaneous images (projections) at 0, 45, 90, and 135° rotations of the collimator. These four acquisitions resulted in paired planar images representing 0/180, 45/225, 90/270, and 135/315° collimator rotational angles. Each acquisition was for 500k producing a total of 2M counts. Total imaging time for the tomographic data was less than 45 min. Image pairs were acquired using a computer‡ into a 128 × 128 byte mode matrix. The eight images were subsequently extracted from the 128 × 128 byte mode matrix and transferred to separate 64 × 64 word mode matrices.

Tomographic reconstruction was performed with CMS software, which utilizes an interative least squares technique (*23*). Reconstruction parameters were selected which produced eight 1.5 cm slices parallel to the collimator face. The slice nearest the camera which demonstrated a lumen within the phantom was called the apical slice,

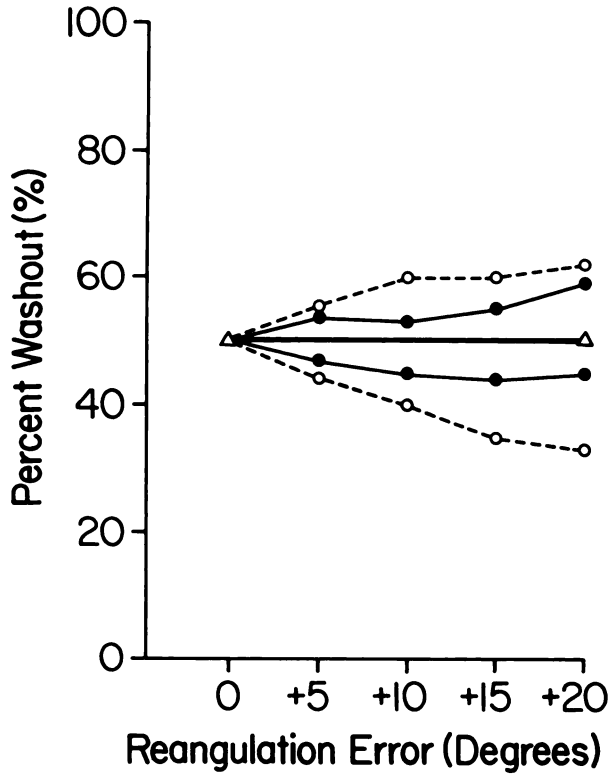

FIGURE 3
No Lesion: This graph represents maximum and minimum percent washout values as function of error in reangulation. These data were derived from washout profile curves in Figure 2B. Maximum and minimum values for both planar and RSH tomographic imaging methods were determined at each angle of error in reangulation and were compared. (○–○) Planar; (•—•) RSH tomography; (Δ—Δ) Expected; $p < 0.05$, Planar vs. tomography

and the subsequent two slices were called the mid and basal slices. The *mid slice* was utilized for comparison with the planar images.

Quantitative techniques

Quantitative circumferential ^{201}Tl activity profile curves for both the planar and reconstructed RSH tomographic mid-slice stress and redistribution images were calculated in the following manner. The center of each image was manually selected and points on the profile were determined by interrogating 60 radials at 6° intervals. The profile values were determined using an algorithm which employed peak count detection, smoothing radially, and smoothing along the profile curve (*23*). The peak search was confined to the points along the radials which best delineated the ^{201}Tl activity in the wall of the phantom. The profile curves were plotted starting at the 3 o'clock position on the image and proceeding in a counterclockwise direction. The radial with the greatest ^{201}Tl activity on the simulated stress image was assigned a value of 100%, and all other points on both the stress and redistribution profile curves were set relative to this value. Each point on the redistribution profile curve was subtracted from the corresponding point on the stress curve, and this quantity was then divided by the corresponding stress point and multiplied by 100 to yield a percent washout of ^{201}Tl activity. The resulting points make up the myocardial ^{201}Tl washout profile curves, which were plotted with the ordinate representing the percent washout of ^{201}Tl activity and the abscissa representing the angle along the profile at 6° radial intervals. Backgound subtraction was not employed in processing either the planar or tomographic images.

Statistical analysis

Maximum positive and negative deviations from the 50% expected percent washout at 0, 5, 10, 15, and 20° angles of mispositioning on the planar and RSH tomographic mid-slice washout profile curves for the no lesion and the lesion top acquisitions were compared using a Wilcoxon rank-sum statistic. The same test procedure was used for the lesion side acquisitions except deviations were assessed at 0, ±5, ±10, ±15, and ±20°. The summed absolute deviations from the 50% expected for all 60 radials on the planar and RSH tomographic washout profile curves for each angle of mispositioning were com-

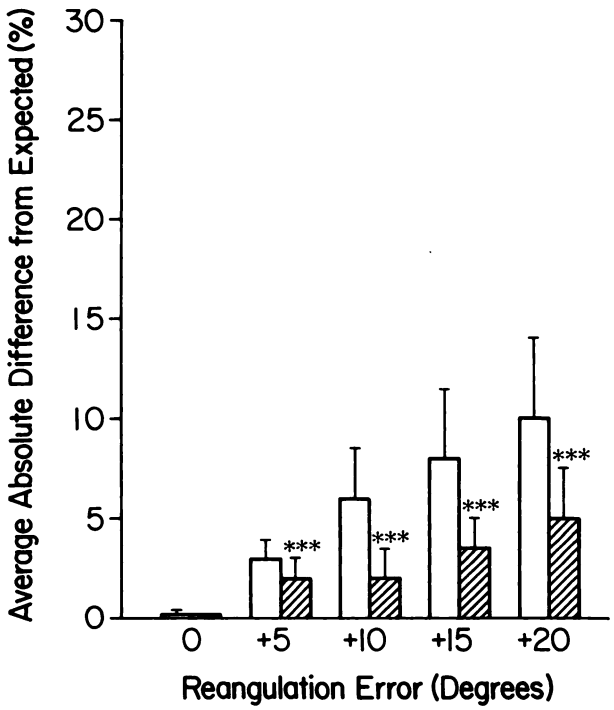

FIGURE 4
No lesion: Bar graphs of mean absolute differences from expected 50% washout are illustrated. These data were derived from the washout profile curves in Fig. 2B. Mean absolute difference was determined by subtraction of observed values from the expected 50% value, by taking absolute difference, summing difference values, and dividing by number of points in curve (60). (□) Planar; (▨) RSH tomography; *** $p < 0.001$; T = + 1 s.d.

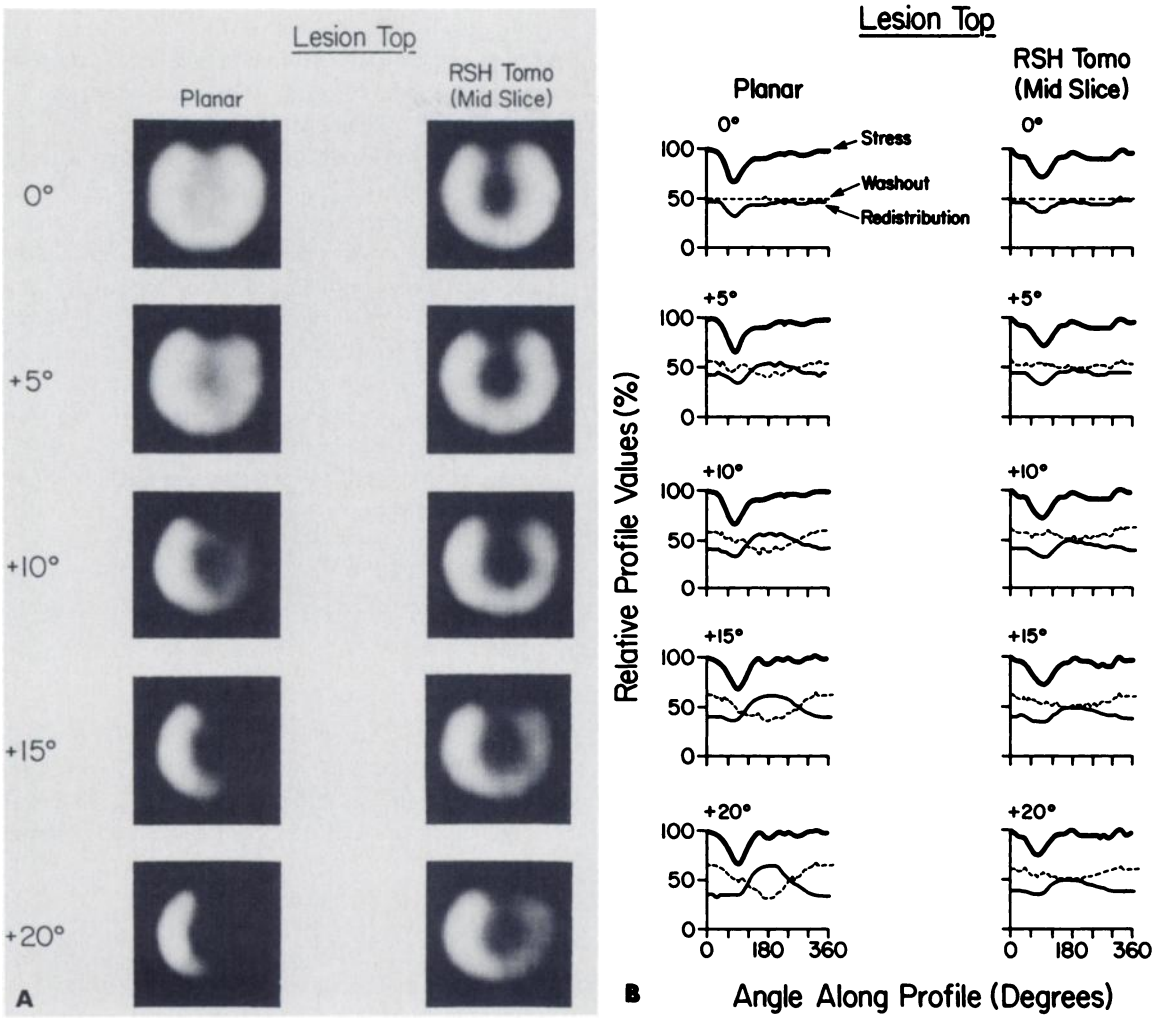

FIGURE 5
A: Planar and RSH tomographic (mid-slice) images of heart phantom containing ^{201}Tl with simulated lesion at top are shown in format similar to Figure 2A
B: Planar and RSH tomographic (mid-slice) stress, redistribution, and washout profile curves from images in Fig. 5A are shown in format similar to Fig. 2B

pared by a two-way analysis of variance. If significant F-statistics were obtained, t-tests were performed at each angle of mispositioning comparing the planar and RSH tomographic values to identify where differences existed. In addition, a one-way analysis of variance and Dunnett's t-tests were performed on the planar and RSH tomographic values to determine at which angle of mispositioning deviations from the expected 50% washout occurred. A probability value of 0.05 or less was considered significant.

RESULTS

No lesion

The effect of tilting the phantom off-axis with no lesion present for both the planar and RSH tomographic mid-slice images is demonstrated in Fig. 2, Panels A and B. The maximum and minimum deviations of the planar and the RSH tomographic washout profile values from the expected 50% washout as a function of the sequential mispositioning of the redistribution phantom are demonstrated graphically in Fig. 3. A significant difference between the planar and tomographic techniques ($p<0.05$), favoring less effect of mispositioning errors on the tomographic images, was demonstrated.

The mean of the absolute differences between the observed and expected 50% washout profile values for all 60 radials for the planar and RSH tomographic techniques at each angle of phantom mispositioning are illustrated in Fig. 4. A significant difference between the mean values was demonstrated when the planar and tomographic studies were compared at each angle of mispositioning ($p<0.001$). This difference, which was more pronounced in the planar studies, was due to misangulation ($p<0.001$)and to the imaging method ($p<0.001$). Also, significant differences from the mean absolute washout

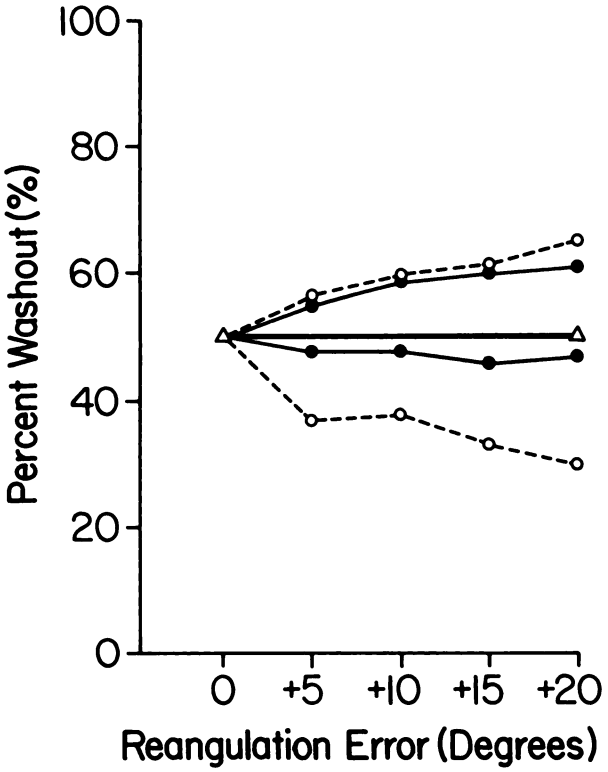

FIGURE 6
Lesion top: This graph represents maximum and minimum percent washout profile values as function of error in reangulation. These data were derived from the washout profile curves of Figure 5B. (○–○) Planar; (•—•) RSH tomography; (Δ—Δ) Expected; $p<0.01$, Planar vs. tomography

profile values at 0° occurred at 5° of misangulation for both the planar and RSH tomographic imaging techniques ($p<0.001$ for both). This difference (relative to the 0° value) progressively increased with increasing misangulation for both the planar and RSH tomographic techniques ($p<0.001$). When adjacent mean absolute values were compared, significant differences occurred ($p<0.001$) for all comparisons, except between the +5° and +10° misangulations for the RSH tomographic technique, where no difference was demonstrated.

Lesion top

The effect of tilting the phantom off axis with a lesion at the top for both the planar and RSH tomographic mid-slice images is demonstrated in Fig. 5, Panels A and B. The maximum and minimum deviations of the planar and the RSH tomographic washout profile values from the expected 50% washout produced by the sequential mispositioning of the redistribution phantom are demonstrated graphically in Fig. 6. A significant difference between the planar and tomographic techniques ($p<0.01$), favoring less effect of mispositioning errors on the tomographic images, was demonstrated.

The mean absolute differences between the observed and expected 50% washout profile values for all 60 radials of the planar and RSH tomographic techniques at each angle of phantom mispositioning are illustrated in Fig. 7. A significant difference between the mean values was demonstrated when the planar and tomographic studies were compared at each angle of mispositioning ($p<0.1$ to 0.001). This difference, which was more pronounced on the planar studies, was due to misangulation ($p<0.001$). Also, significant differences from the mean absolute washout profile values at 0° occurred at 5° of misangulation for both the planar and RSH tomographic imaging techniques ($p<0.001$ for both). This difference (relative to the 0° value) progressively increased with increasing misangulation for both the planar and RSH tomographic techniques ($p<0.001$). When adjacent mean absolute values were compared, significant differences occurred ($p<0.001$) for all comparisions except between the +10, and +15° and the +15 and +20° misangulations for the RSH tomographic technique, where no differences were demonstrated.

Lesion side

The effect of tilting the phantom off axis with a lesion at the side (left) for both the planar and RSH tomographic mid-slice images is demonstrated in Fig. 8, Panels A and B. The maximum and minimum deviations of the planar

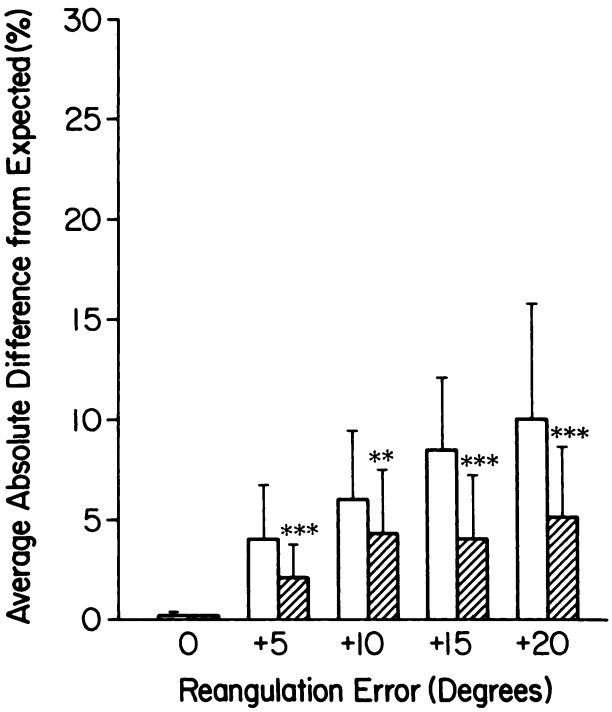

FIGURE 7
Lesion top: Bar graphs of mean absolute difference from expected 50% percent washout are illustrated. These data were derived from the washout profile curves in Figure 5B. (□) Planar; (▨) RSH tomography; ** $p<0.01$; *** $p<0.01$; T = + 1 s.d.

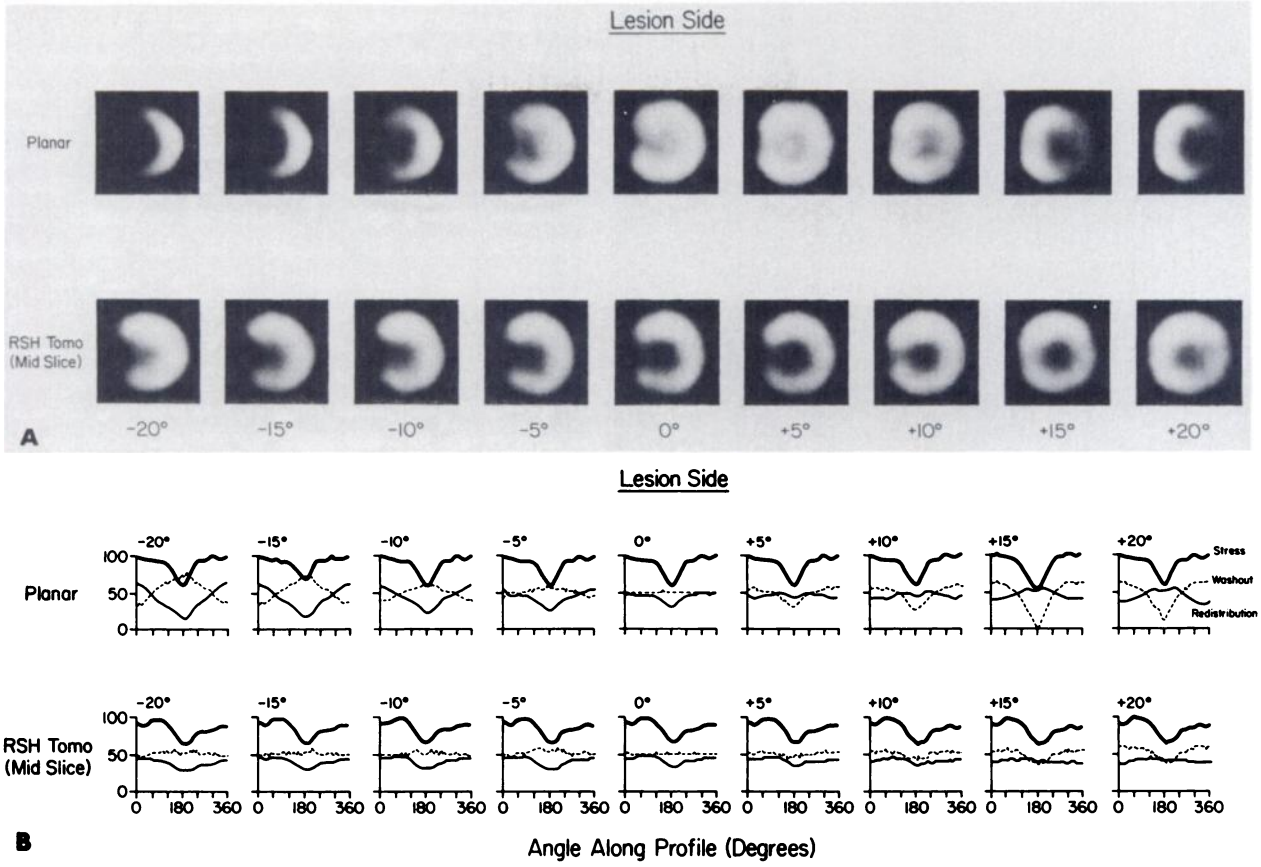

FIGURE 8
Upper: Planar and RSH tomographic (mid-slice) images of heart phantom containing Tl-201 with simulated lesion on left are shown in manner similar to Fig. 2A
Lower: Planar and RSH tomographic (mid-slice) stress, redistribution, and washout profile curves from images in Fig. 8A are shown in manner similar to Fig. 2B

and the RSH tomographic washout profile values from the expected 50% washout produced by the sequential mispositioning of the redistribution phantom are demonstrated graphically in Fig. 9. A significant difference between the planar and tomographic techniques ($p<0.001$), favoring less effect of mispositioning errors on the tomographic images, was demonstrated.

The mean absolute differences between the observed and expected 50% washout profile values for all 60 radials of the planar and the RSH tomographic techniques at each angle of phantom mispositioning are illustrated in Fig. 10. A significant difference between the mean values was demonstrated when the planar and tomographic studies were compared at each angle of mispositioning ($p<0.05$ to 0.001). This difference, which was more pronounced on the planar studies, was due to misangulation ($p<0.001$) and to the imaging method ($p<0.001$). Also, significant differences from the mean absolute washout profile values at 0° occurred at +5° as well as -5° of misangulation for both the planar and RSH tomographic imaging techniques ($p<0.001$ for both). This difference (relative to the 0° value) progressively increased with

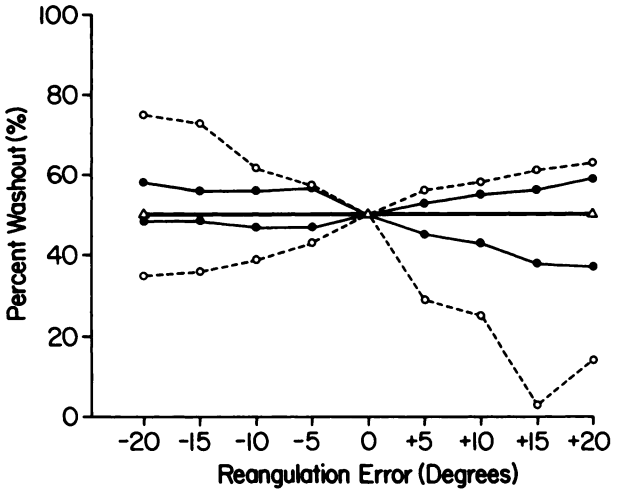

FIGURE 9
Lesion side: This graph represents maximum and minimum percent washout profile values as function of error in reangulation. These data were derived from washout profile curves in Figure 8B. (○–○) Planar; (•—•) RSH tomography; (Δ—Δ) Expected; $p<0.001$ positive, negative, Planar vs. tomography

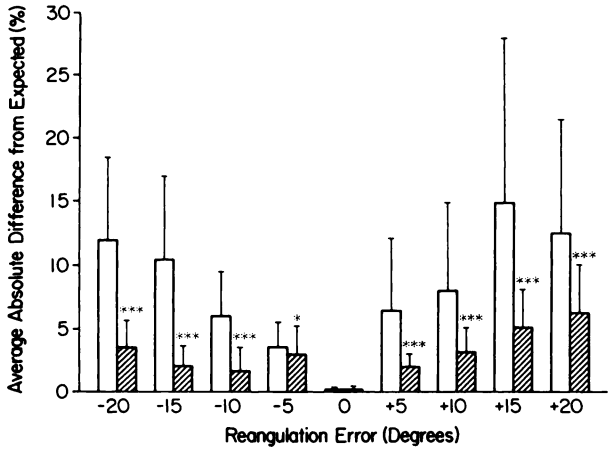

FIGURE 10
Lesion side: Bar graphs of mean absolute difference from expected 50% washout are illustrated. These data were derived from the washout profile curves in Figure 8B. □ Planar; ▨ RSH tomography; * $p<0.05$; *** $p<0.001$; T = + 1 s.d.

increasing misangulation for both the planar and RSH tomographic techniques ($p<0.001$). When adjacent mean absolute values for the planar technique were compared, significant differences occurred ($p<0.001$) for all comparisons except between the +5 and +10° and the +15 and +20° misangulations, where no significant differences were demonstrated. No significant differences were seen for the adjacent comparisions from -5 to -20° misangulations for the RSH tomographic technique.

Washout profiles in the lesions

The maximum and minimum deviations of the planar and RSH tomographic washout profile values from the expected 50% washout in the lesions produced by the sequential mispositioning of the redistribution phantoms are shown in Fig. 11. A significant difference between the planar and tomographic techniques ($p<0.01$), favoring less effect of mispositioning errors on the tomographic images, is demonstrated.

DISCUSSION

Qualitative ^{201}Tl myocardial scintigraphy is now a well-established noninvasive method for diagnosing coronary artery disease (*1–8*). Because of certain well-defined limitations, including observer variability in the interpretation of planar images (*24*), and problems identifying high risk lesions such as left main or three-vessel disease (*25–27*), quantitative techniques have been developed. Quantitative ^{201}Tl methods have been reported to be superior to qualitative planar imaging in detecting three-vessel disease and identifying specific vessel involvement (*9,10*).

Another limitation of both qualitative and quantitative planar ^{201}Tl myocardial scintigraphy is related to the image display and background subtraction (*28*). This, in part, led to the application of tomographic technology to ^{201}Tl myocardial imaging. The three forms of tomography, which have been applied to ^{201}Tl myocardial imaging, are seven-pinhole collimator (*13–16*), rotating slant hole (RSH) collimator (*22,23*), and rotating camera or transaxial tomography (*17,18,20*). Seven-pinhole ^{201}Tl myocardial scintigraphy compares favorably with planar ^{201}Tl myocardial scintigraphy (*13,16*), but it has been criticized for not demonstrating true cross-sectional activity and introducing artifactual defects (*29,30*). Ratib and coauthors reported RSH tomographic ^{201}Tl imaging to be more sensitive than planar imaging for detecting myocardial defects, but they also noted the occurrence of artifactual defects due to positioning problems in the axial direction (*31*). Finally, transaxial tomographic ^{201}Tl imaging has been reported to be superior to planar ^{201}Tl imaging for detecting myocardial infarction qualitatively (*32*). Although tomographic ^{201}Tl myocardial scintigraphy may eliminate some of the problems one must consider with planar imaging, it, like qualitative and quantitative planar imaging, is subject to artifacts in the images due to mispositioning errors.

Our data shows that a photopenic defect becomes progressively more apparent in the wall of the redistribution planar and RSH tomographic images tilted towards the camera surface as the angle of the mispositioning is increased. This effect was more pronounced with the planar images than with the RSH tomographic images at each point of misangulation of the redistribution phantom. The corresponding redistribution profile curves demonstrate

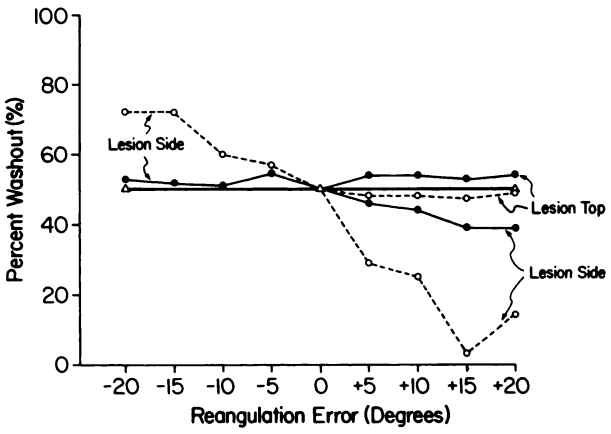

FIGURE 11
Washout profile values in location of lesion for data with simulated lesion positioned at top and side of phantom are shown. These values are averages of three washout profile values centered on 90° profile angle for the lesion top curves and the 180° profile angle for lesion side (left) curves. Lesion top profile curve data were only evaluated for positive angles, while the lesion side data were evaluated for positive and negative tilt angles. (○–○) Planar; (•—•) RSH tomography; (Δ—Δ) Expected; $p<0.01$ positive; negative

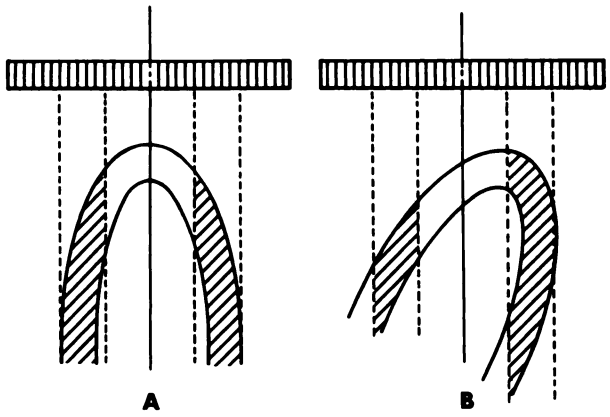

FIGURE 12
Diagrammatic representation of planar acquisition using parallel-hole collimator with correct positioning (A) and incorrect positioning (B) is illustrated

this phenomena. Also, a relative increase in ^{201}Tl activity was noted in the wall opposite to the photopenic defect with increasing misangulation of the redistribution phantom. The quantitative washout profile curves decreased when the redistribution profile curves increased and vice versa. There was a false increase in percent washout in the wall of the redistribution phantom which was tilted toward the camera surface and a false decrease on the opposite side. As with the qualitative images, the relative effect on the washout profile curves was more pronounced on the planar compared to the RSH tomographic images, with each increase in misangulation of the redistribution phantom. Furthermore, similar data were obtained from the planar and RSH tomographic mid-slice images when a lesion was present.

A partial explanation for the artifactual defects developing with angulation of the heart phantom is illustrated in Figs. 12 and 13. In Fig. 12, Panel A, the long axis of the phantom is perpendicular to the camera surface; and the planar ^{201}Tl activity pattern is symmetrical. However, in Fig. 12, Panel B, the phantom is tilted off-axis; and the corresponding areas of the camera crystal would detect different amounts of ^{201}Tl activity resulting in an asymmetrical planar image. This would also explain how erroneous washout profile data could result if the stress and redistribution phantoms were not realigned at the same axial angle. Figure 13, Panels A and B, demonstrate that the volumes of activity for the RSH tomographic system are more nearly equal for the mispositioned phantom than for the planar system. This more restrictive volume sampling partially explains why the ^{201}Tl washout profile values with this tomographic system are less affected by misangulation of the phantom than are the planar washout profile values.

We chose to simulate the 0° tilt images as comparable 45° LAO projections with the long axis of the left ventricle aligned perpendicular to the plane of the collimator in this investigation for both the planar and tomographic imaging acquisitions. This orientation is, in fact, the one which yields the least distortion in reconstructed RSH tomographic planes (*30,31*) and, therefore, it is the desired reference orientation. Also, this orientation is used in all qualitative methods since the circumferential washout profile curves represent the tissue perfused by the three major coronary arteries. The differences we observed between the planar and RSH tomographic images in the standard LAO reference orientation may diminish for small angles of reangulation error when other views (anterior or lateral) are taken as the reference orientation. Additionally, the effects observed with the CMS heart phantom are partially due to the geometry of this phantom, which has relatively steep walls. In the clinical setting the effects of errors in reangulation are probably less severe due to the more elliptical shape of the left ventricle. Since the effects of reangulation errors have been shown to be less for RSH tomographic imaging than for comparable LAO planar imaging, tomographic techniques for ^{201}Tl imaging of the left ventricle are suggested.

The clinical implication of this study, similar to that reported by Ratib et al. (*31*), is that the sensitivity and specificity of quantitative planar and RSH tomographic ^{201}Tl myocardial imaging are probably decreased when the heart is imaged with the long axis of the left ventricle positioned off the perpendicular to the camera surface. The present investigation shows that this problem is more pronounced with planar imaging for any angle of mispositioning. It also demonstrates that any change in the position of the heart in the axial direction between the stress and redistribution acquisitions may lower the sensitivity and specificity of quantitative washout profile analysis for both the planar and tomographic techniques. Chang and

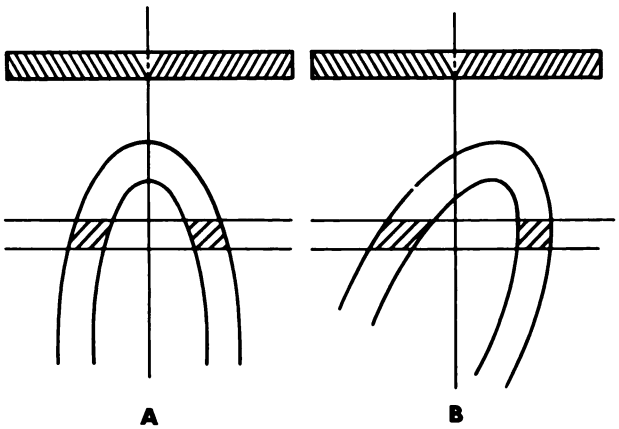

FIGURE 13
Diagrammatic representation of tomographic acquisition and reconstructed mid-slice using bilateral RSH collimator with correct positioning (A) and incorrect positioning (B) are illustrated

Henkin (*33*) reported that alignment of the long axis of the left ventricle can be achieved within +/- 10° with a quadrant slant-hole (QSH) collimator. In a similar way, we have used the 0 and 90° image pairs of the CMS bilateral RSH collimator for alignment in a clinical study which demonstrated good sensitivity and specificity of the washout profile curves for coronary artery disease (*23*).

In conclusion, RSH tomographic ^{201}Tl quantitative washout profile curves are less subject to off-axis reangulation artifacts than comparable planar quantitative analysis. This study emphasizes the need for meticulous attention to detail in repositioning patients between the stress and redistribution ^{201}Tl myocardial image acquisitions. Accurate repositioning will minimize the contribution of reangulation artifacts to quantitative ^{201}Tl percent washout profile analysis irrespective of the method of ^{201}Tl myocardial imaging clinically employed.

FOOTNOTES

*Cardiac Medical Systems (CMS), Inc., Springfield, WI.

†Picker Dynamo, Picker International, Northford, CT.

‡Medtronic A2 computer, MDS Ann Arbor, MI. (out of business)

§MEDX, Inc., Rolling Meadows, IL.

ACKNOWLEDGMENTS

The authors acknowledge the technical assistance of Betty Heyl, Suzanne Patrick-Fischer, and Heather Varnnum. Dr. Starling is supported by NIH Research Career Development Award #K04-HL01446 from the National Heart, Lung and Blood Institute, Bethesda, MD.

This work was supported in part by NIH New Investigator Research Award #R23-HL27508 and #R01-HL32845 from the National Heart, Lung and Blood Institute, Bethesda, MD.

REFERENCES

1. Bailey IK, Griffith LSC, Rouleau J, et al: Thallium-201 myocardial perfusion imaging at rest and during exercise. *Circulation* 55:79-87, 1977
2. Ritchie JL, Trobaugh GB, Hamilton GW, et al: Myocardial imaging with thallium-201 at rest and during exercise. *Circulation* 56:66-71, 1977
3. Verani MS, Marcus ML, Razzak MA, et al: Sensitivity and specificity of thallium-201 perfusion scintigrams under exercise in the diagnosis of coronary artery disease. *J Nucl Med* 19:773-782, 1978
4. Botvinick EH, Taradash MR, Shames DM, et al: Thallium-201 myocardial perfusion scintigraphy for the clinical clarification of normal, abnormal and equivocal electrocardiographic stress tests. *Am J Cardiol* 41:43-51, 1978
5. Ritchie JL, Albro PC, Caldwell JH, et al: Thallium-201 myocardial imaging: A comparison of the redistribution and rest images. *J Nucl Med* 20:477-483, 1979
6. Verani MS, Jhingran S, Attar M, et al: Poststress redistribution of thallium-201 in patients with coronary artery disease, with and without prior myocardial infarction. *Am J Cardiol* 43:1114-1122, 1979
7. Leppo J, Yipintsoi T, Blankstein R, et al: Thallium-201 myocardial scintigraphy in patients with triple-vessel disease and ischemic exercise stress tests. *Circulation* 59:714-721, 1979
8. Iskandrian AB, Segal BL: Value of exercise thallium-201 imaging in patients with diagnostic and nondiagnostic exercise electrocardiograms. *Am J Cardiol* 48:233-238, 1981
9. Berger BC, Watson DD, Taylor GJ, et al: Quantitative thallium-201 exercise scintigraphy for detection of coronary artery disease. *J Nucl Med* 22:585-593, 1981
10. Maddahi J, Garcia EV, Berman DS, et al: Improved noninvasive assessment of coronary artery disease by quantitative analysis of regional stress myocardial distribution and washout of thallium-201. *Circulation* 64:924-935, 1981
11. Garcia E, Maddahi J, Berman D, et al: Space/time quantitation of thallium-201 myocardial scintigraphy. *J Nucl Med* 22:309-317, 1981
12. Watson DD, Campbell NP, Read EK, et al: Spatial and temporal quantitation of plane thallium myocardial images. *J Nucl Med* 22:577-584, 1981
13. Vogel RA, Kirch DL, LeFree MT, et al: Thallium-201 myocardial perfusion scintigraphy: Results of standard and multi-pinhole tomographic techniques. *Am J Cardiol* 43:787-793, 1979
14. Williams DL, Ritchie JL, Harp GD, et al: In vivo simulation of thallium-201 myocardial scintigraphy by seven-pinhole emission tomography. *J Nucl Med* 21:821-828, 1980
15. Ritchie JL, Williams DL, Caldwell JH, et al: Seven-pinhole emission tomography with thallium-201 in patients with prior myocardial infarction. *J Nucl Med* 22:107-112, 1981
16. Rizi JR, Kline RC, Thrall JH, et al: Thallium-201 myocardial scintigraphy: A critical comparison of seven-pinhole tomography and conventional planar imaging. *J Nucl Med* 22:493-499, 1981
17. Tamaki N, Mukai T, Ishii Y, et al: Comparative study of thallium emission myocardial tomography with 180° and 360° data collection. *J Nucl Med* 23:661-666, 1982
18. Ritchie JL, Williams DL, Harp G, et al: Transaxial tomography with thallium-201 for detecting remote myocardial infarction. *Am J Cardiol* 50:1236-1241, 1982
19. Kirsch CM, Doliwa R, Buell U, et al: Detection of severe coronary heart disease with Tl-201: Comparison of resting single photon emission tomography with invasive arteriography. *J Nucl Med* 24:761-767, 1983
20. Tamaki N, Yonekura Y, Mukai T, et al: Stress thallium-201 transaxial emission tomography: Quantitative versus qualitative analysis for evaluation of coronary artery disease. *J Am Coll Cardiol* 4:1213-1221, 1984
21. Garcia EV, Van Train K, Maddahi J, et al: Quantification of rotational thallium-201 myocardial tomography. *J Nucl Med* 26:17-26, 1985
22. Starling MR, Dehmer GJ, Lancaster JL, et al: Segmental coronary artery disease: Detection by rotating slant-hole collimator tomography and planar thallium-201 myocardial scintigraphy. *Radiology*: in press
23. Lasher JC, Blumhardt R, Kopp DT, et al: Emission computed tomography: Versatile limited angle software. In *Emission Computed Tomography: Current Trends*, Esser PD, ed. New York, Society of Nuclear Medicine, 1981, pp 211-225
24. Atwood JE, Jensen D, Froelicher V, et al: Agreement in human interpretation of analog thallium myocardial perfusion images. *Circulation* 64:601-609, 1981

25. Dash H, Massie BM, Botvinick EH, et al: The noninvasive identification of left main and three-vessel coronary artery disease by myocardial stress perfusion scintigraphy and treadmill exercise electrocardiography. *Circulation* 60:276-284, 1979
26. Rigo P, Bailey IK, Griffith SC, et al: Value and limitations of segmental analysis of stress thallium myocardial imaging for localization of coronary artery disease. *Circulation* 61:973-981, 1980
27. Hör G, Kanemoto N: Thallium-201 myocardial scintigraphy: Current status in coronary artery disease results of sensitivity/specificity in 3092 patients and clinical recommendations. *J Nucl Med* 20:136-147, 1981
28. Goris M: Nontarget activities: Can we correct them? *J Nucl Med* 20:1312-1314, 1979
29. Tamaki N, Mukai T, Ishii Y, et al: Clinical evaluation of thallium-201 emission myocardial tomography using a rotating gamma camera: Comparison with seven-pinhole tomography. *J Nucl Med* 22:849-855, 1981
30. Budinger TF: Physical attributes of single-photon tomography. *J Nucl Med* 21:579-592, 1980
31. Ratib O, Henze E, Hoffman E, et al: Performance of the rotating slant-hole collimator for the detection of myocardial perfusion abnormalities. *J Nucl Med* 23:34-41, 1982
32. Maublant J, Cassagnes J, LeJeune J, et al: A comparison between conventional scintigraphy and emission tomography with thallium-201 in the detection of myocardial infarction: Concise communication. *J Nucl Med* 23:204-208, 1982
33. Chang W and Henkin RE: Performance of the rotating slant-hole collimator for the detection of myocardial perfusion abnormalities. (lett) *J Nucl Med* 23:547, 1982